THE ASTROPHYSICAL JOURNAL, 363:554–573, 1990 November 10

HOT AND COLD GAS TOWARD YOUNG STELLAR OBJECTS

GEORGE F. MITCHELL,[1,2,3] JEAN-PIERRE MAILLARD,[3,4] MARK ALLEN,[3,5]
REINHARD BEER,[3,5] AND KENNETH BELCOURT[1]
Received 1990 February 2; accepted 1990 May 9

ABSTRACT

High-resolution ($\lambda/\Delta\lambda = 37{,}000$) M band (4.7 μm) spectra are presented for the seven embedded infrared sources W3 IRS 5, S140 IRS 1, NGC 7538 IRS 1, NGC 7538 IRS 9, GL 2136, LkHα 101, and MWC 349A. Absorption lines of the fundamental vibrational band of ^{12}CO are seen in all of the sources, and corresponding ^{13}CO lines are detected in five. Other spectral features seen are (1) blueshifted ^{12}CO absorption in five of the seven sources; (2) clear ^{12}CO *emission* lines in two sources (S140 IRS 1 and NGC 7538 IRS 9), and possible CO emission lines in two others (W3 IRS 5 and NGC 7538 IRS 1); (3) hydrogen recombination lines in two sources (LkHα 101 and MWC 349A); (4) CO ($v = 1$–2) absorption lines in one source, GL 2136; and (5) broad absorption at 2140 cm^{-1}, due to solid CO, in W3 IRS 5, NGC 7538 IRS 1, and NGC 7538 IRS 9. Analysis of the CO lines yields values for the gas temperature and column density in the line of sight to each source. Results from the above seven objects are combined with our previously published results for W33A and GL 2591 to make a sample of nine objects. Although blueshifted CO absorption (i.e., outflowing gas) is seen in six of the nine objects, we discuss in this paper only the quiescent (i.e., nonoutflowing) gas.

Cold gas is seen toward all sources, with temperature from 11 K (for MWC 349A) to 66 K (for W3 IRS 5). Eight of the nine sources show, in addition, hot gas, with temperature from 120 K (for W33A) to 1010 K (for GL 2591). The cold gas resides in the molecular cloud within which the objects are embedded. The gas temperatures of the cold component agree very well with temperatures deduced from emission lines at millimeter and centimeter wavelengths. For five of the lines of sight, ^{13}CO column densities calculated from the infrared absorption lines are in quite good agreement with ^{13}CO column densities calculated from radio emission lines, given the uncertainties inherent in the use of emission lines (e.g., beam dilution and self-absorption). The location of the hot gas component, and its heat source, is uncertain. We present arguments in favor of the view that the hot gas toward GL 2591, GL 2136, W3 IRS 5, and S140 IRS 1 is very near the embedded object and is heated via gas-grain collisions. For the sources NGC 7538 IRS 1, NGC 7538 IRS 9, LkHα 101, and W33A, the same model may apply, but the clumpy cloud picture presented by Harris *et al.* in 1987, in which ultraviolet photons from nearby hot stars penetrate and heat the gas, cannot be excluded.

The ratio of solid to gaseous CO is obtained for seven sources, using solid CO abundances published by Sandford *et al.* in 1988. The fraction of CO in solid form is quite high for the sources NGC 7538 IRS 9 and W33A (4% and 10%, respectively). The four other lines of sight have less than 1% of CO in the solid state.

Subject headings: interstellar: molecules — infrared: spectra — stars: pre–main-sequence

I. INTRODUCTION

The properties of molecular clouds are most commonly studied by the observation of emission lines arising from the deexcitation of collisionally excited molecules. Species that are widely used as probes of molecular clouds include CO, CS, NH_3, and HCO^+. Transparent (i.e., diffuse) interstellar clouds have been successfully studied for many years by absorption spectroscopy in the ultraviolet and visible, using background hot stars as sources of illumination. The exploitation of near-infrared (1–5 μm) absorption spectroscopy as a probe of molecular clouds and cloud cores, using embedded (or background) infrared objects, has begun only relatively recently. Much of the published work has been at only moderate resolution ($\lambda/\Delta\lambda \approx 1000$), and most of the high-resolution work has been restricted to relatively narrow spectral bands. The use of both high spectral resolution ($\lambda/\Delta\lambda > 10^4$) and broad wavelength coverage has the obvious advantage of permitting the simultaneous measurement of many molecular lines in a given band. The power of high spectral resolution, broad band, infrared spectroscopy as a probe of molecular cloud cores was convincingly demonstrated by Scoville *et al.* (1983) in their study of the BN object in Orion, employing the Fourier Transform Spectrometer at the Kitt Peak 4 m telescope. The same instrument was used by Black and Willner (1984) in a study of NGC 2024.

In this paper we present results from an observing program carried out at the Canada-France-Hawaii Telescope on Mauna Kea using the Fourier Transform Spectrometer at the Cassegrain focus. We have observed lines of the fundamental vibrational band of CO at 4.7 μm toward embedded young stellar objects. Some results of the program, emphasizing newly detected outflows, have been published (Mitchell *et al.* 1988*a*, *b*; Mitchell, Allen and Maillard 1988; Mitchell *et al.* 1989). Here we discuss the properties of the quiescent gas toward nine YSOs.

The nine sources in this study do not, by any means, form a homogeneous sample. They can be divided into three groups. The five objects GL 2591, S140 IRS 1, W3 IRS 5, NGC 7538 IRS 1, and NGC 7538 IRS 9 are luminous, deeply embedded, and are sources of spatially extended gas outflows. These five

[1] Department of Astronomy, Saint Mary's University, Halifax.
[2] Visiting Scientist, the Canada-France-Hawaii Telescope Corporation, Waimea, Hawaii.
[3] Visiting Astronomer, Canada-France-Hawaii Telescope, operated by the NRC of Canada, the CNRS of France, and the University of Hawaii.
[4] Institut d'Astrophysique, Paris.
[5] Earth and Space Sciences Division, Jet Propulsion Laboratory, Pasadena.

are classical examples of objects which were, until recently, called protostars but which are now, more cautiously, denoted young stellar objects. The two sources W33A and GL 2136 are also luminous and highly reddened but they do not show evidence of gas outflow. They appear in lists of YSOs but their status is not clear. The two objects LkHα 101 and MWC 349A are very different from the other seven in being much less deeply embedded in gas and dust. They are emission-line objects, probably at or near the zero-age main sequence. The evolutionary status of MWC 349A is controversial. White and Becker (1985) suggest that it is an evolved object. Hamann and Simon (1988), on the other hand, stress the similarities between MWC 349A and young stellar objects. They model MWC 349A as a rotating disk plus a bipolar wind.

In § II below, spectra of the individual sources, showing ^{12}CO and ^{13}CO lines, are presented. Gas temperatures and column densities are calculated in § III, where it is shown that both hot and cold gas is often seen. In § IV the infrared temperatures and column densities are compared with available millimeter emission line measurements. A strong correlation between CO column density and silicate optical depth is demonstrated in § V. In § VI a comparison is made between solid and gaseous CO abundance for six lines of sight. The location and heating of the hot gas component are discussed in § VII, and conclusions of the paper are reiterated in § VIII.

II. THE OBSERVATIONS

The data were obtained in 1987 July and 1988 September/October using the Fourier Transform Spectrometer on the Canada-France-Hawaii Telescope. A log of the observations is given in Table 1. A filter with a bandpass of ≈ 100 cm^{-1}, centered on 2130 cm^{-1} (4.695 (μm), was employed. In each case, a resolution of $\lambda/\Delta\lambda = 37{,}000$ was used, corresponding, at 4.7 μm, to a velocity resolution of 8 km s^{-1} (full width at half-maximum). Beam-switching of the source between the two entrance apertures was used to cancel the thermal background. Removal of absorption lines formed in Earth's atmosphere is effected by ratioing the source spectrum with that of a standard star. The standard should be of early spectral type to ensure the absence of molecular absorption lines in its atmosphere. For each source, we used the A0 star, α Lyr, as the standard. On the same night that each source was observed, a spectrum of α Lyr was obtained through a similar air mass. Preliminary data processing, resulting in co-added spectra, was done at CFHT headquarters in Waimea. The measurement of line positions, widths, and equivalent widths was carried out at Saint Mary's University using interactive software written by K. Belcourt. The software was validated by comparison with extensive measurements of the GL 2591 spectrum made by hand, using ruler and planimeter.

TABLE 1

LOG OF THE OBSERVATIONS

Source	Date	Integration Time (minutes)
GL 2136	1987 Jul 11	128
W3 IRS 5	1988 Sep 30	96
S140 IRS 1	1987 Jul 12	160
	1988 Sep 30	224
NGC 7538 IRS 1	1988 Oct 2	144
NGC 7538 IRS 9	1988 Oct 1	160
LkHα 101	1988 Oct 2	40
MWC 349A	1987 Jul 10	80

Figure 1 shows a typical spectrum of α Lyr to illustrate the sky spectrum in the bandpass. The intensity scale in Figures 1–8 is in arbitrary units. Telluric ^{12}CO lines, from *P*15 to *R*8, are labelled in Figure 1. The FTS spectra are subject to channeling, a sinusoidal modulation of the intensity caused by internal reflection in the cold filters. Some of the apparent structure in the α Lyr spectrum on a scale of ≈ 1 cm^{-1} is, in fact, due to channeling. Because of channeling, the continuum of the source and the standard star must be carefully matched in the vicinity of the line of interest before a ratio is taken. The ragged appearance of the spectrum in the *P* branch, at wavenumbers below 2130 cm^{-1} (Fig. 1*a*), is due to telluric N_2O absorption. The *R* branch (Fig. 1*b*) is much cleaner, containing well-separated lines of H_2O and CO.

Spectra of the sources GL 2136, W3 IRS 5, S140 IRS 1, NGC 7538 IRS 1, NGC 7538 IRS 9, LkHα 101, and MWC 349A are shown in Figures 2 through 8. In each spectrum, CO (0–1) absorption lines are detected with velocities at or near the velocity of the respective molecular cloud core, as previously found from CO emission at millimeter wavelengths. Other spectral features seen are (1) blueshifted ^{12}CO absorption in five of the seven sources; (2) clear ^{12}CO *emission* lines in two sources (S140 IRS 1 and NGC 7538 IRS 9), and possible CO emission lines in two others (W3 IRS 5 and NGC 7538 IRS 1); (3) hydrogen recombination lines in two sources (LkHα 101 and MWC 349A); (4) CO ($v = 1$–2) absorption lines in one source, GL 2136; and (5) broad absorption at 2140 cm^{-1}, due to solid CO, in W3 IRS 5, NGC 7538 IRS 1, and NGC 7538 IRS 9. The present paper is concerned with the quiescent (i.e., rest velocity) gas. The outflows and emission features will be discussed in future publications.

Figure 2 shows the uncorrected spectrum of GL 2136. Detected lines of ^{12}CO are labeled above the spectrum. At the date of observation, the Doppler shift of GL 2136 relative to Earth was fairly small (19 km s^{-1} or 0.14 cm^{-1}), so that telluric CO lines, indicated by the symbol ⊕, are partially blended with the interstellar ^{12}CO lines. The component to the left is the interstellar component. As well as being blended with telluric lines, the ^{12}CO lines are strongly saturated and cannot be used to deduce gas properties. The corresponding lines of ^{13}CO are also present and are not saturated. The ^{13}CO lines are labeled below the spectrum. In addition, 12 absorption lines arising from CO in the first excited vibrational level are seen in the spectrum, making GL 2136 the second source we have observed (after GL 2591; Mitchell *et al.* 1989) which shows vibrationally excited CO lines. The CO($v = 1$–2) lines are denoted by an asterisk in Figure 2.

The spectrum of W3 IRS 5 is shown in Figure 3. The absorption lines of ^{12}CO, labeled above the spectrum, show four velocity components, one at the velocity of the cloud core and three blueshifted with respect to the cloud core. The CO absorption consists, morphologically, of two broad features each with two components. The total velocity range of the absorption is ≈ 60 km s^{-1}. The quiescent absorption, discussed in this paper, is the reddest (lowest wavenumber) component of the four. The interstellar absorption lines are well separated from the telluric CO lines (denoted by ⊕) by a large Doppler shift. Narrow CO emission lines, to the red of the absorption lines are likely present. The emission lines appear strongest in the *P*-branch, particularly *P*11, *P*9, and *P*8. A spectrum with a higher signal-to-noise ratio is needed to

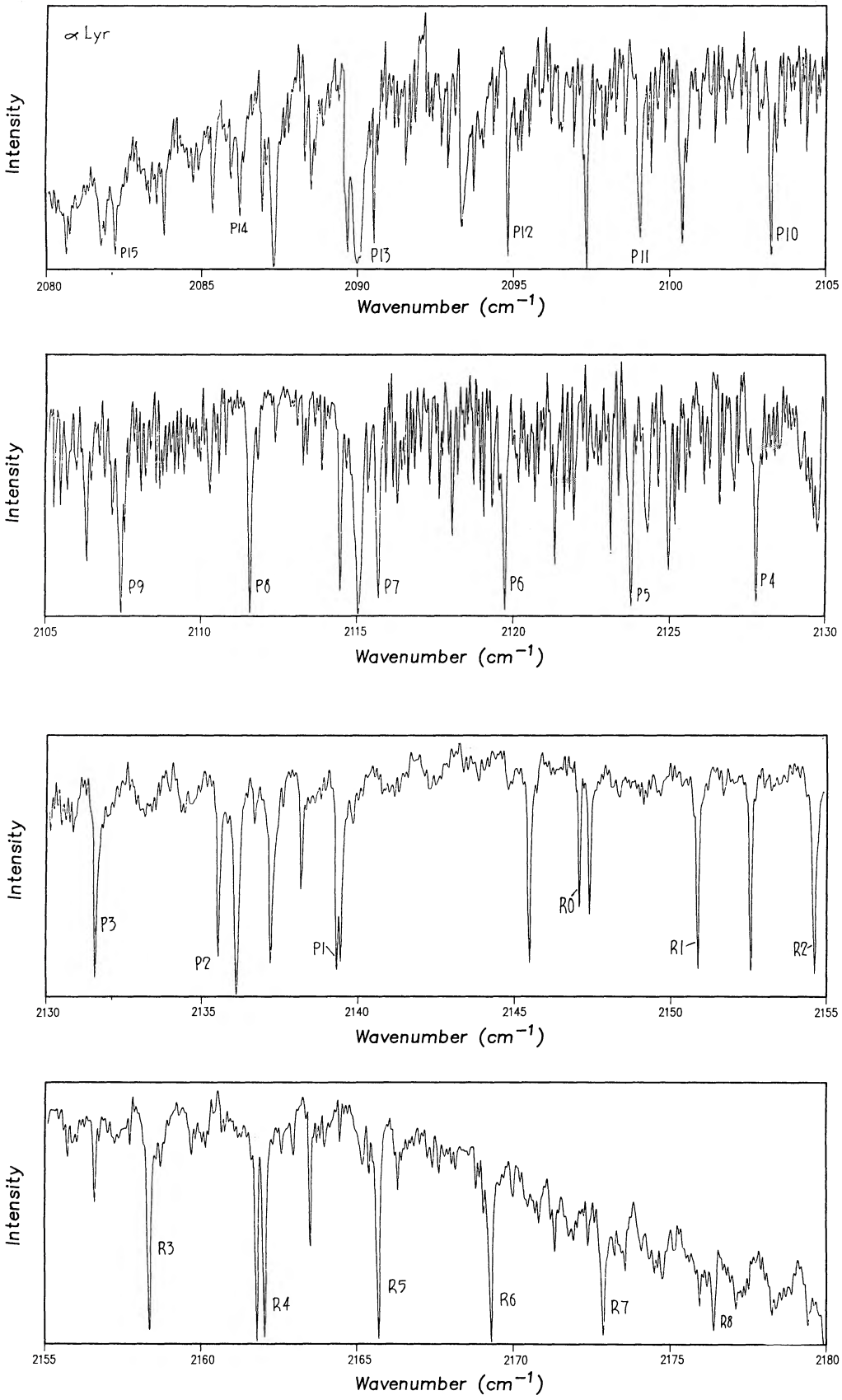

FIG. 1.—The spectrum of the standard star, α Lyr, illustrates the spectrum of the sky in our bandpass. Telluric lines, from *P*15 through *R*8, are labeled. The intensity scale is in arbitrary units.

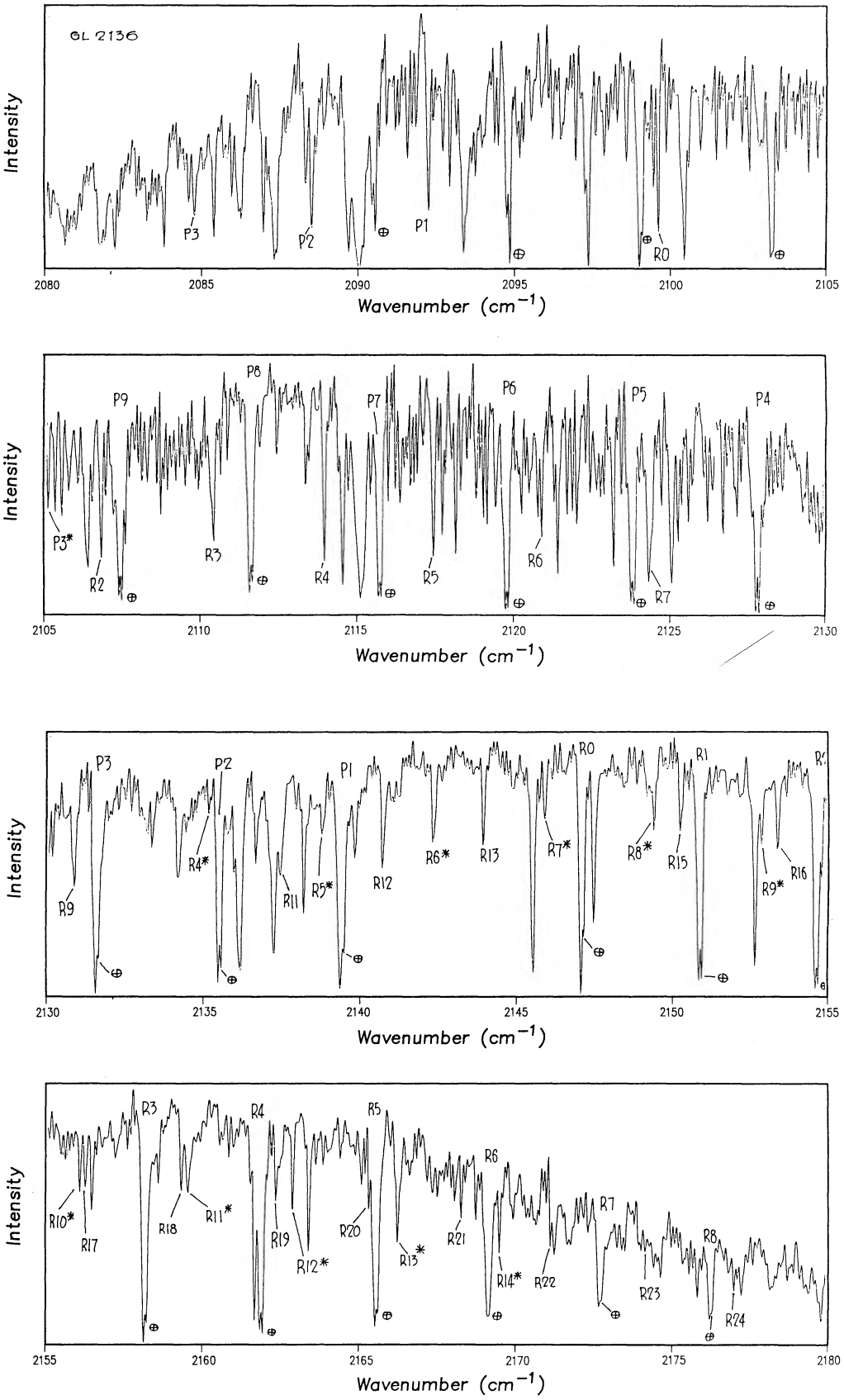

FIG. 2.—The spectrum of GL 2136, uncorrected for absorption due to Earth's atmosphere. Absorption lines of ^{12}CO are labeled above the spectrum and absorption lines of ^{13}CO are labeled below. The telluric lines of ^{12}CO are denoted by the symbol $\oplus$. $^{12}CO(v = 1–2)$ lines are denoted by an asterisk.

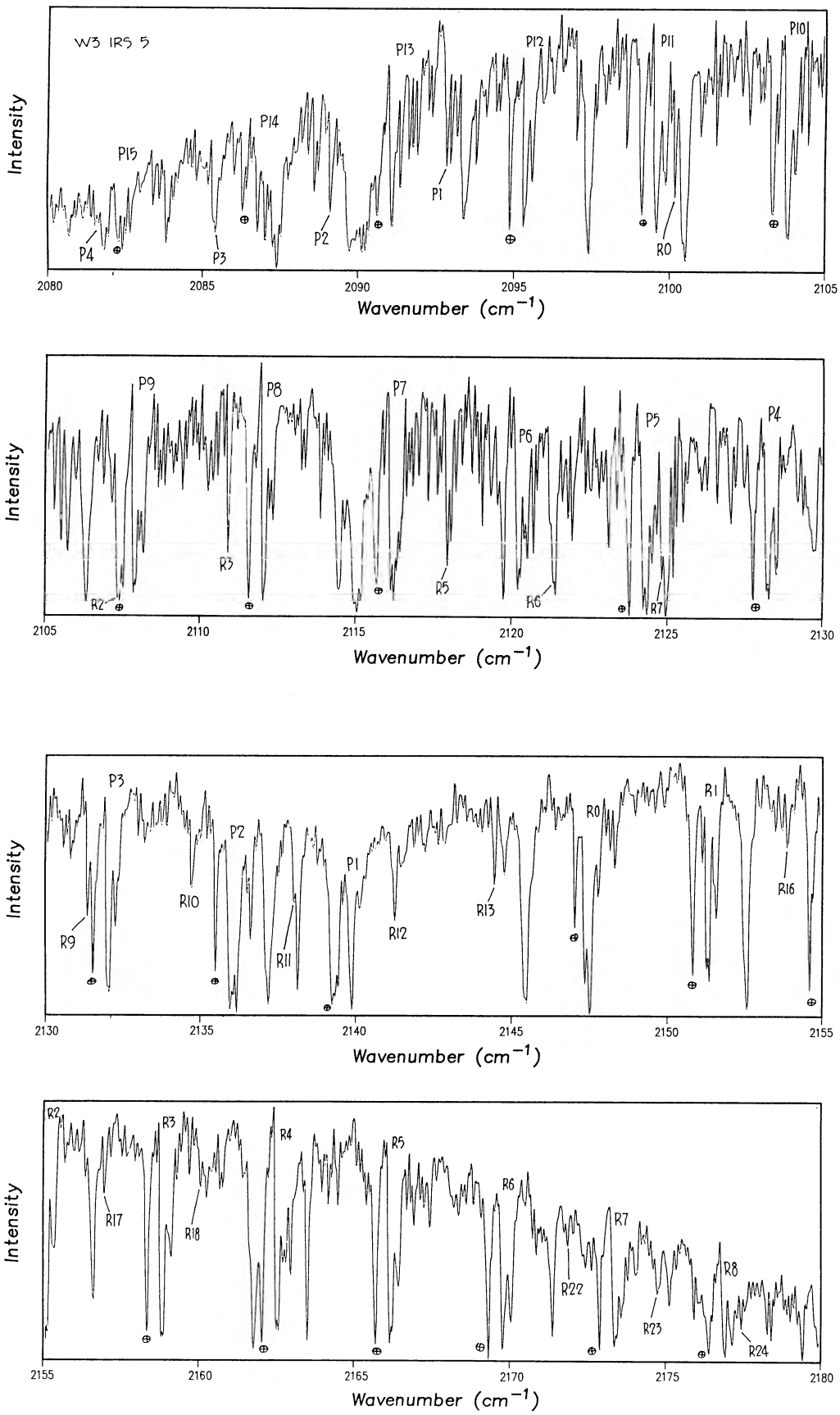

FIG. 3.—The same as Fig. 2 but for W3 IRS 5

confirm their existence in this source. Absorption lines of ^{13}CO at the source velocity are detected and are labeled below the spectrum. Previous results for W3 IRS 5, presented in Mitchell *et al.* (1990), were based on a spectrum of W3 IRS 5 having only half the signal-to-noise ratio of the spectrum in Figure 3. The gas properties for W3 IRS 5 deduced in this paper are consistent with, but not identical to, the properties presented earlier. The results presented in this paper supersede those of Mitchell *et al.* (1990).

Figure 4 shows the spectrum of S140 IRS 1. Strong ^{12}CO absorption lines are present and are labeled above the spectrum. Emission lines of ^{12}CO are very clear in this source. The emission is redshifted by ≈ 10 km s^{-1} relative to the absorption, so that the CO lines are P Cygni in character. At the resolution of 8 km s^{-1}, the emission lines are unresolved. The ^{12}CO absorption lines are asymmetrical, having a blue wing which can be interpreted as gas outflowing at a velocity of 12 km s^{-1}. ^{13}CO absorption lines corresponding to the ^{12}CO lines are present and are labeled below the spectrum.

The spectrum of NGC 7538 IRS 1 (Fig. 5) shows strong ^{12}CO lines at the source velocity. A blueshifted wing to the ^{12}CO absorption lines indicates gas outflowing at a velocity of ≈ 10 km s^{-1}. Narrow, redshifted ^{12}CO emission is probably present, although weak. Absorption lines of ^{13}CO from *P*4 through *R*13 are present and are labeled below the spectrum.

NGC 7538 IRS 9 (Fig. 6) exhibits two strong interstellar absorption components due to ^{12}CO. The redder component is at the velocity of the cloud core, while the other component is blueshifted by 16 km s^{-1}. As in S140 IRS 1, strong, narrow emission lines of ^{12}CO are present to the red of the rest velocity absorption, giving P Cygni–like CO profiles. The blueshifted CO absorption lines have a pronounced wing to the blue and are consistent with two blended velocity components having outflow velocities of 16 and 28 km s^{-1} relative to the source. The very broad absorption feature centered at 2140 cm^{-1} is due to solid CO. NGC 7538 IRS 9 has the deepest solid CO absorption of any source observed to date. In the solid CO feature the intensity drops to essentially zero, so that no gas phase absorption lines are measurable in this part of the spectrum (from ≈ 2138 to 2143 cm^{-1}). Despite the strength of the ^{12}CO absorption lines, only low-*J* lines of ^{13}CO, $J \leq 6$, are seen.

The emission-line star LkHα 101 has a much smaller column density of foreground gas than the previous sources. Interstellar ^{12}CO lines are, therefore, weaker. Sixteen ^{12}CO lines are present (Fig. 7), with values of the rotational quantum number up to $J = 6$. They are labeled below the spectrum. No ^{13}CO lines are detectable. The Pfβ recombination line of hydrogen at 2149 cm^{-1}, formed in an outflowing ionized wind, is very strong. Its full width at half maximum is 42 km s^{-1}, consistent with that of the Brγ line (Simon and Cassar 1984). Note that the intensity scale in the portion of Figure 7 containing Pfβ is compressed in order to accommodate the emission.

Only that portion of the spectrum of MWC 349A (Fig. 8) is displayed which shows interstellar features. Four weak ^{12}CO absorption lines are seen, namely the *R*0, *P*1, *R*1, and *R*3 lines. No ^{13}CO is detected. The two hydrogen recombination lines Pfβ (7–6) and Huϵ (11–6), are very strong. These are the only H lines which fall in the filter bandpass. The emission lines are asymmetric and broad, consistent with other recombination lines observed in this source (e.g., Hamann and Simon 1986). The Pfβ line, measured after ratioing, has a FWHM of 92 km s^{-1}, a FWZI of 157 km s^{-1}, and an equivalent width of 1.015 cm^{-1}. The Huϵ line has a FWHM of 111 km s^{-1}, a FWZI of 160 km s^{-1}, and an equivalent width of 0.232 cm^{-1}.

TABLE 2

CLOUD CORE VELOCITIES: INFRARED ABSORPTION COMPARED WITH MILLIMETER EMISSION

OBJECT	v_{LSR} (km s^{-1}) Infrared	v_{LSR} (km s^{-1}) Millimeter	REFERENCE TO MILLIMETER v_{LSR}
W33A	32.6 ± 1.7	36	1
W3 IRS 5	−42.4 ± 1.5	−39	2
GL 2136	26.5 ± 2.8	27.2	3
GL 2591	−10.7 ± 0.4	−6	4
NGC 7538/1	−59.2 ± 1.2	−58	5
NGC 7538/9	−59.7 ± 1.9	−58	5
S140 IRS 1	−8.5 ± 1.0	−8.5	6
LkHα 101	−0.3 ± 0.5	−1.2	7
MWC 349A	3.1 ± 1.7	−3.5	8

REFERENCES.—(1) Goldsmith and Mao 1983; (2) Hayashi *et al.* 1989; (3) Dinger *et al.* 1979; (4) Bally and Lada 1983; (5) Kameya *et al.* 1989; (6) Margulis and Lada 1985; (7) Redman *et al.* 1986; (8) Knapp *et al.* 1977.

The velocities of all CO lines were measured from ratioed spectra. Velocities with respect to the local standard of rest (v_{LSR}) of the quiescent cloud core component are given in Table 2, where they are compared with velocities of CO emission lines at millimeter wavelengths. Velocities obtained from the ^{13}CO lines are used for the seven sources with ^{13}CO lines. The ^{13}CO lines, being narrower, give greater accuracy. For each source, the velocity listed in Table 2 is the average over all measured lines, and the error is a measure (1 σ) of the scatter in the individual measurements. The infrared and millimeter velocities agree to within 2 σ for seven of the sources. In the case of GL 2591, the difference is larger, as pointed out previously (Mitchell *et al.* 1989). For MWC 349A, the discrepancy is greater than 3 σ, possibly suggesting an error (typographical?) in the millimeter velocity tabulated by Knapp *et al.* (1977).

III. CALCULATIONS OF GAS PROPERTIES

For an optically thin line, the column density of CO in the initial rotational state of the transition, N_J, can be found directly from the equivalent width using the relation

$$W_\omega = \frac{\pi e^2}{m_e c^2} f_J N_J$$

where W_ω is the equivalent width in cm^{-1}, f_J is the absorption oscillator strength of the transition, and the other symbols have their usual meanings. For the objects W33A, W3 IRS 5, GL 2136, NGC 7538 IRS 1, NGC 7538 IRS 9, and S140 IRS 1, the rest-velocity ^{12}CO lines are saturated and cannot be used to obtain column densities. For the above sources, however, ^{13}CO lines are reasonably strong and are not saturated, so that ^{13}CO column densities can be found. In the spectra of LkHα 101 and MWC 349A, on the other hand, ^{13}CO lines are not seen, but ^{12}CO lines are detected and are not saturated, so that ^{12}CO column densities can be obtained for these objects. Measured equivalent widths of ^{13}CO and ^{12}CO lines are listed in Tables 3 and 4. In the case of S140 IRS 1, the tabulated widths are averages of the 1987 July and 1988 September observations.

Because the ^{13}CO ($v = 0$–1) lines are not always optically thin for sources as deeply embedded as these (e.g., Scoville *et al.* 1983; Mitchell *et al.* 1989), we cannot assume the optically thin

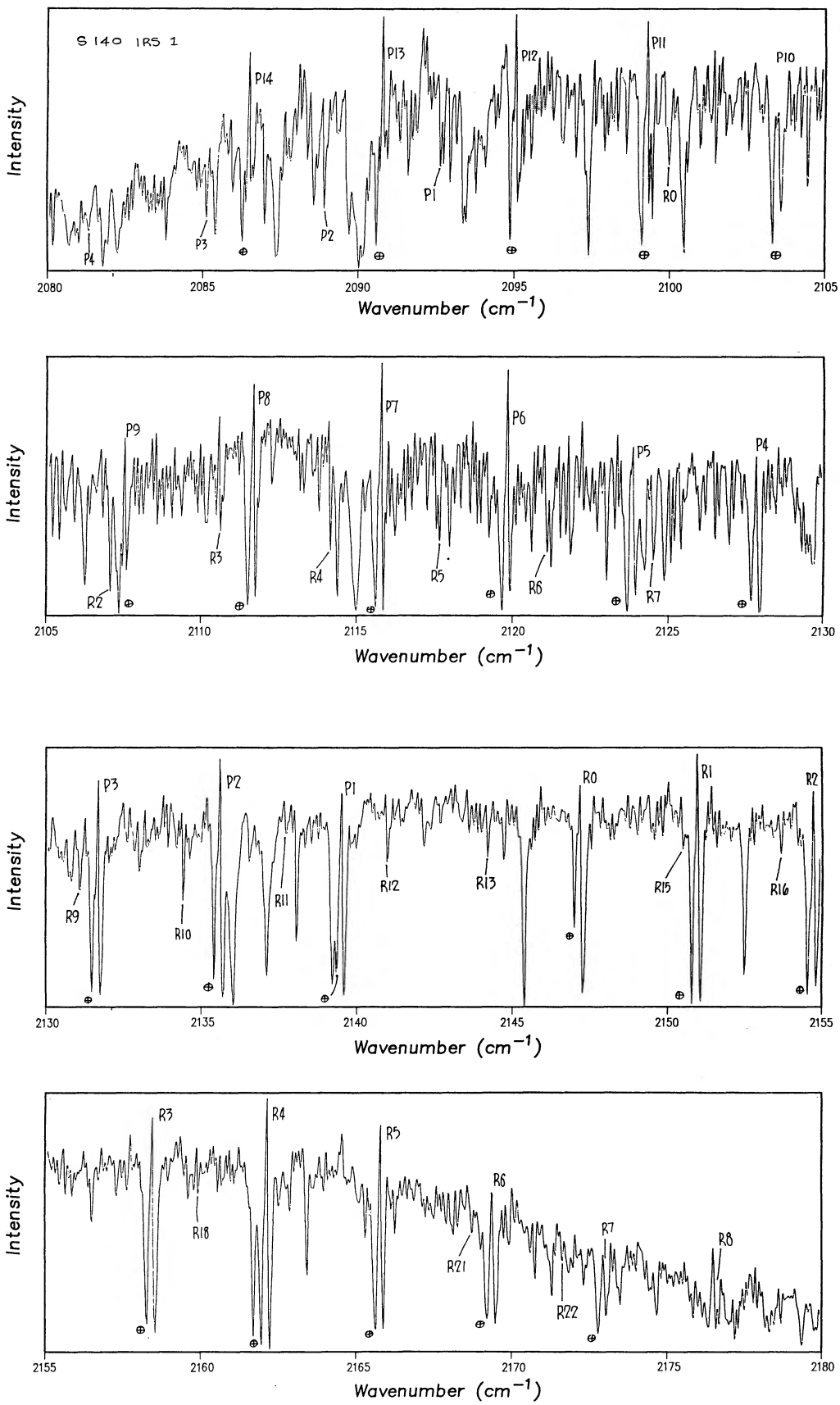

FIG. 4.—The same as Fig. 2 but for S140 IRS 1. In addition to absorption lines of ^{12}CO and ^{13}CO, emission lines of ^{12}CO are strong in this source.

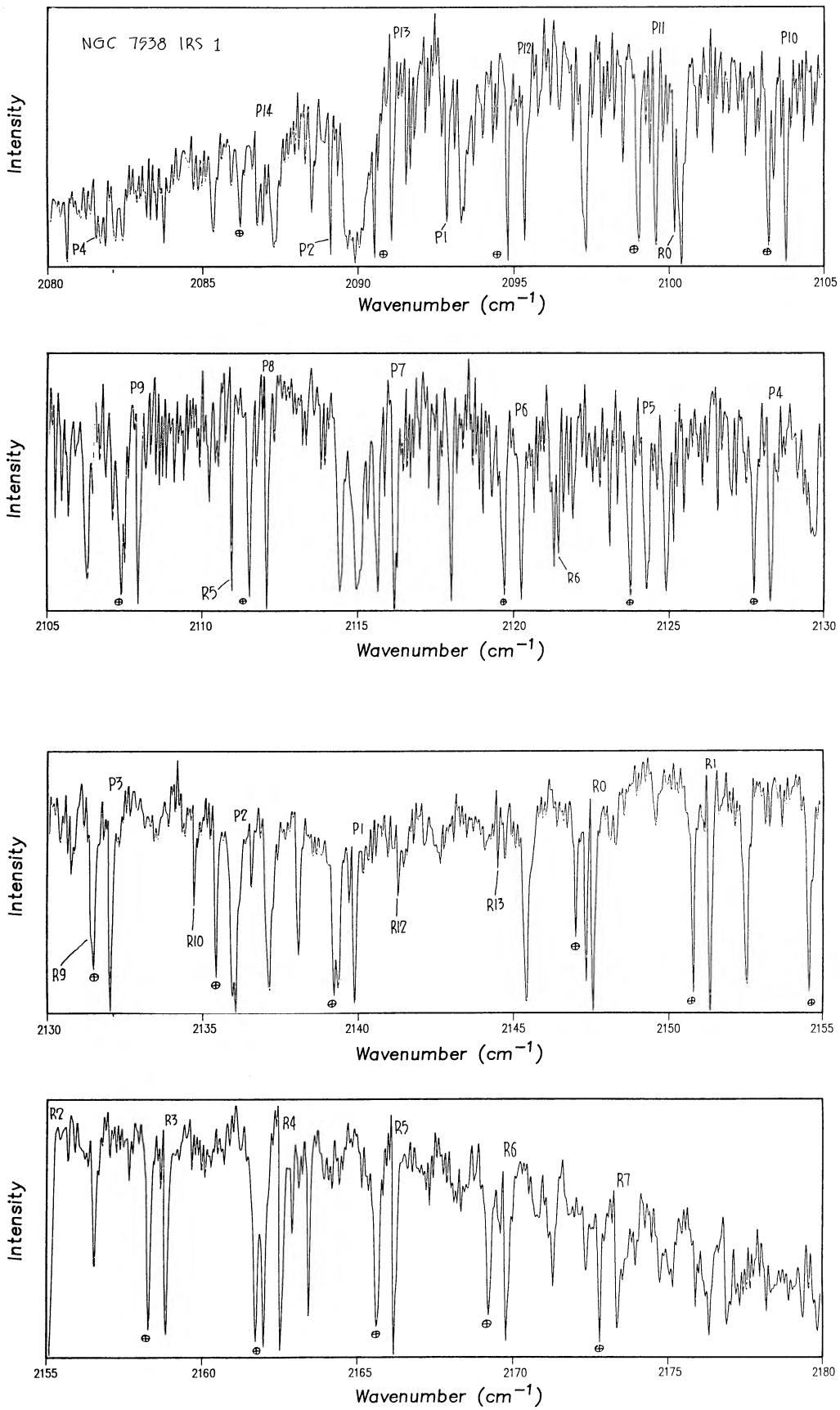

FIG. 5.—The same as Fig. 2 but for the source NGC 7538 IRS 1

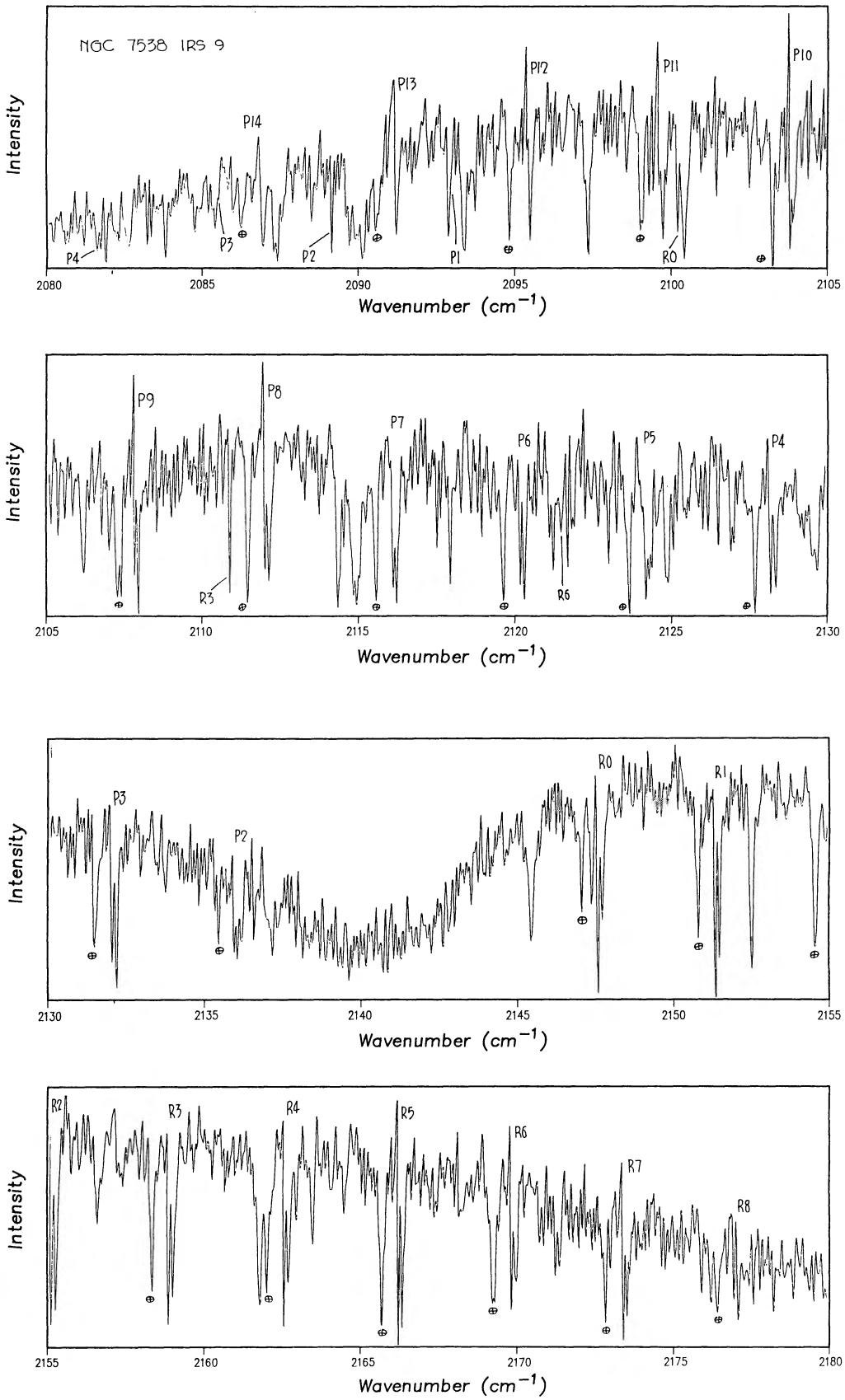

FIG. 6.—The same as Fig. 2 but for NGC 7538 IRS 9. In addition to absorption lines of ^{12}CO and ^{13}CO, emission lines of ^{12}CO are strong. The broad absorption feature centered at 2140 cm^{-1} is due to solid CO.

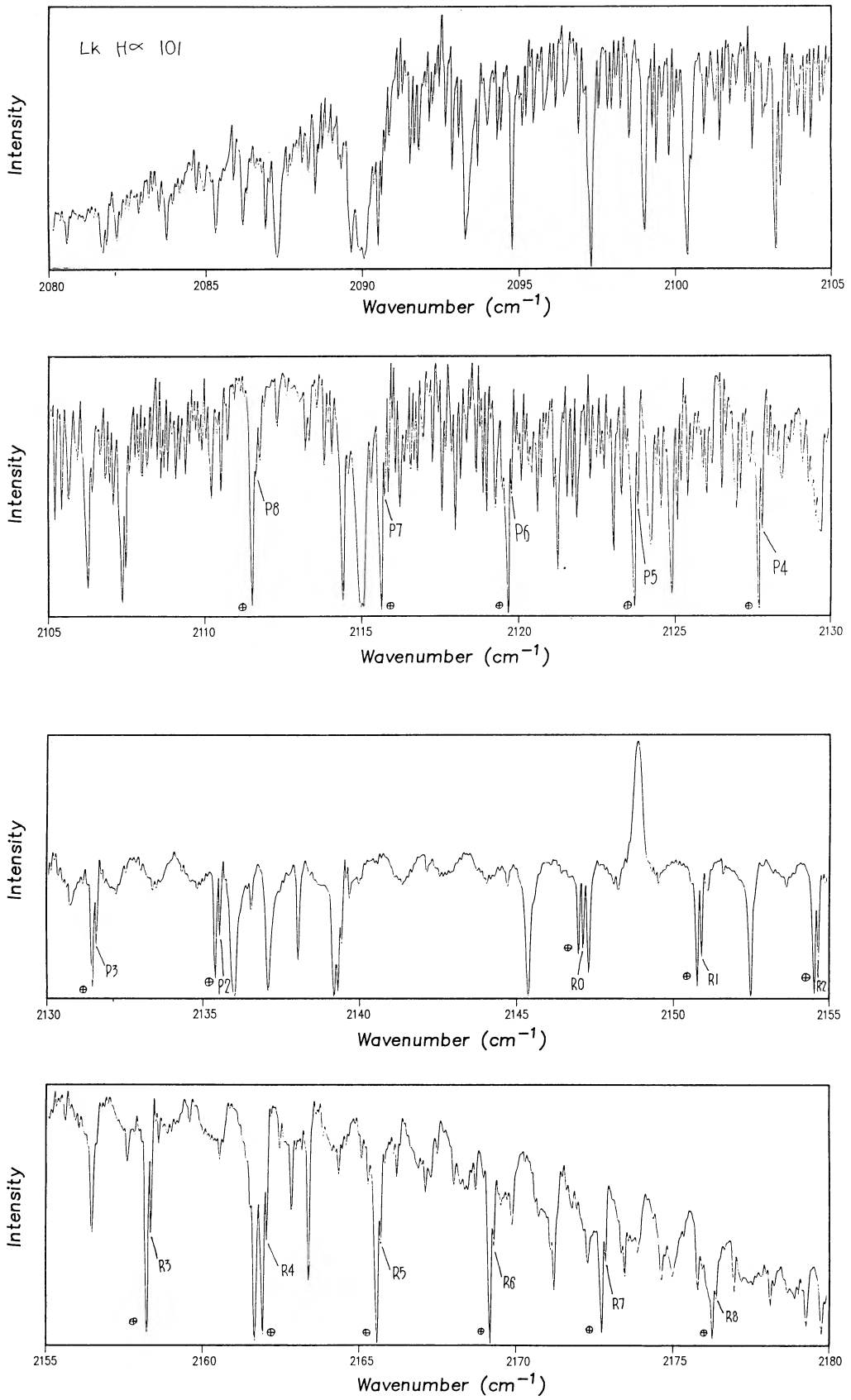

FIG. 7.—The spectrum of LkHα 101. Lines of ^{12}CO, from *P*8 to *R*8, are labeled below the spectrum. The corresponding telluric lines are denoted by the symbol ⊕. The Pfund-β emission line of hydrogen is labeled.

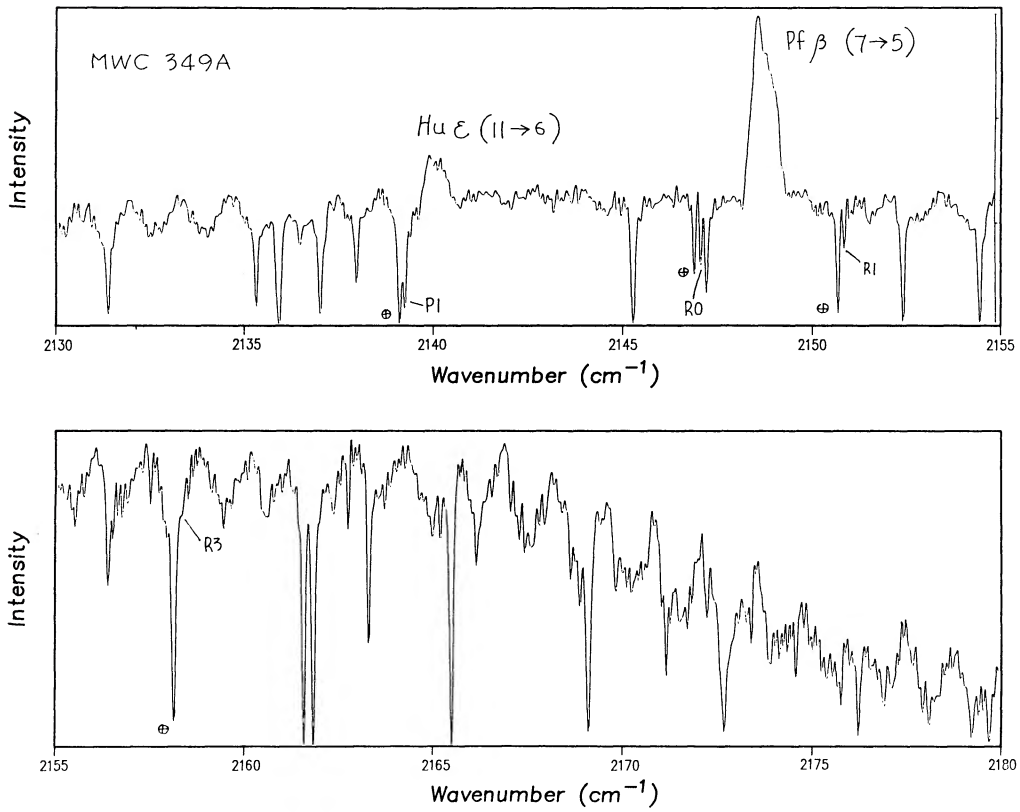

FIG. 8.—A portion of the spectrum of MWC 349A. The *P*1, *R*0, *R*1, and *R*3 interstellar lines of ^{12}CO are labeled. Two hydrogen recombination lines, the Pfund-β and the Humphreys-ϵ lines, are shown.

relation connecting W_ω and N_J but must carry out a curve-of-growth analysis. For each source, it is necessary to adopt an appropriate line width (FWHM). The averaged measured ^{13}CO line width in each source is 10–12 km s^{-1}. After correction for an instrumental width of 8 km s^{-1}, the intrinsic line widths should be 6.5–9 km s^{-1}. We feel, however, that the ^{13}CO lines are, at best, marginally resolved, and that widths obtained in this way cannot reliably be used in a curve-of-growth analysis. It is probably significant that the mean line width in all the sources is similar and is only slightly larger than the instrumental width: noise will inevitably increase line widths to values exceeding the nominal resolution. A second indication that the lines are not resolved is the fact that the high-*J* lines and low-*J* lines in each spectrum have the same

TABLE 3

EQUIVALENT WIDTHS OF ^{13}CO LINES (cm^{-1})

Line	W3 IRS 5	GL 2136	NGC 7538/1	NGC 7538/9	S140/1
*R*0.....	0.0656	0.0571	0.0597	0.0583	0.0338
*P*1.....	0.0551	0.0820	0.0645	0.0728	0.0385
*R*2.....	0.0820	0.0688	...	...	0.0468
*P*2.....	0.0667	0.0682	0.0800	0.0710	0.0366
*R*3.....	0.0573	0.0518	0.0745	0.0727	0.0429
*P*3.....	0.0547	0.0490	...	0.0274	0.0376
*R*4.....	...	0.0704	...	...	0.0410
*P*4.....	0.0529	...	0.0417	0.0728	0.0356
*R*5.....	0.0639	0.0699	...	...	0.0269
*R*6.....	0.0650	0.0432	0.0486	0.0097	0.0308
*R*7.....	0.0514	0.0561	...	...	0.0288
*R*9.....	0.0451	0.0384	0.0340	...	0.0223
*R*10.....	0.0368	...	0.0330	...	0.0208
*R*11.....	0.0275	0.0449	...	...	0.0218
*R*12.....	0.0437	0.0504	0.0205	...	0.0187
*R*13.....	0.0375	0.0409	0.0152	...	0.0165
*R*15.....	0.0352	0.0288	...	...	0.0139
*R*16.....	0.0353	0.0275	...	...	0.0124
*R*17.....	0.0320	0.0305	...	...	0.0103
*R*18.....	0.0136	0.0395	...	...	0.0092
*R*19.....	...	0.0311	...	...	0.0076
*R*20.....	0.0194	0.0157	...	...	...
*R*21.....	...	0.0252	...	...	...
*R*22.....	0.0160	0.0295	...	...	...
*R*23.....	0.0108	0.0216	...	...	...
*R*24.....	0.0173	0.0016	...	...	...

TABLE 4

EQUIVALENT WIDTHS OF ^{12}CO LINES (cm^{-1})

Line	NGC 7538/9	LkHα 101	MWC 349A
*R*0.....	0.0935	0.0445	0.0376
*R*1.....	0.0977	0.0436	0.0264
*P*1.....	...	...	0.0103
*R*2.....	0.0866	0.0311	...
*P*2.....	...	0.0385	...
*R*3.....	0.0735	0.0337	0.0080
*P*3.....	0.0534	0.0397	...
*R*4.....	0.0574	0.0347	...
*P*4.....	0.0643	0.0305	...
*R*5.....	0.0672	0.0223	...
*P*5.....	0.0573	0.0225	...
*R*6.....	0.0565	0.0256	...
*P*6.....	0.0654	0.0189	...
*R*7.....	0.0669	...	...
*P*7.....	...	0.0162	...
*R*8.....	0.0502	0.0238	...
*P*8.....	0.0551	0.0076	...
*P*9.....	0.0492	...	...

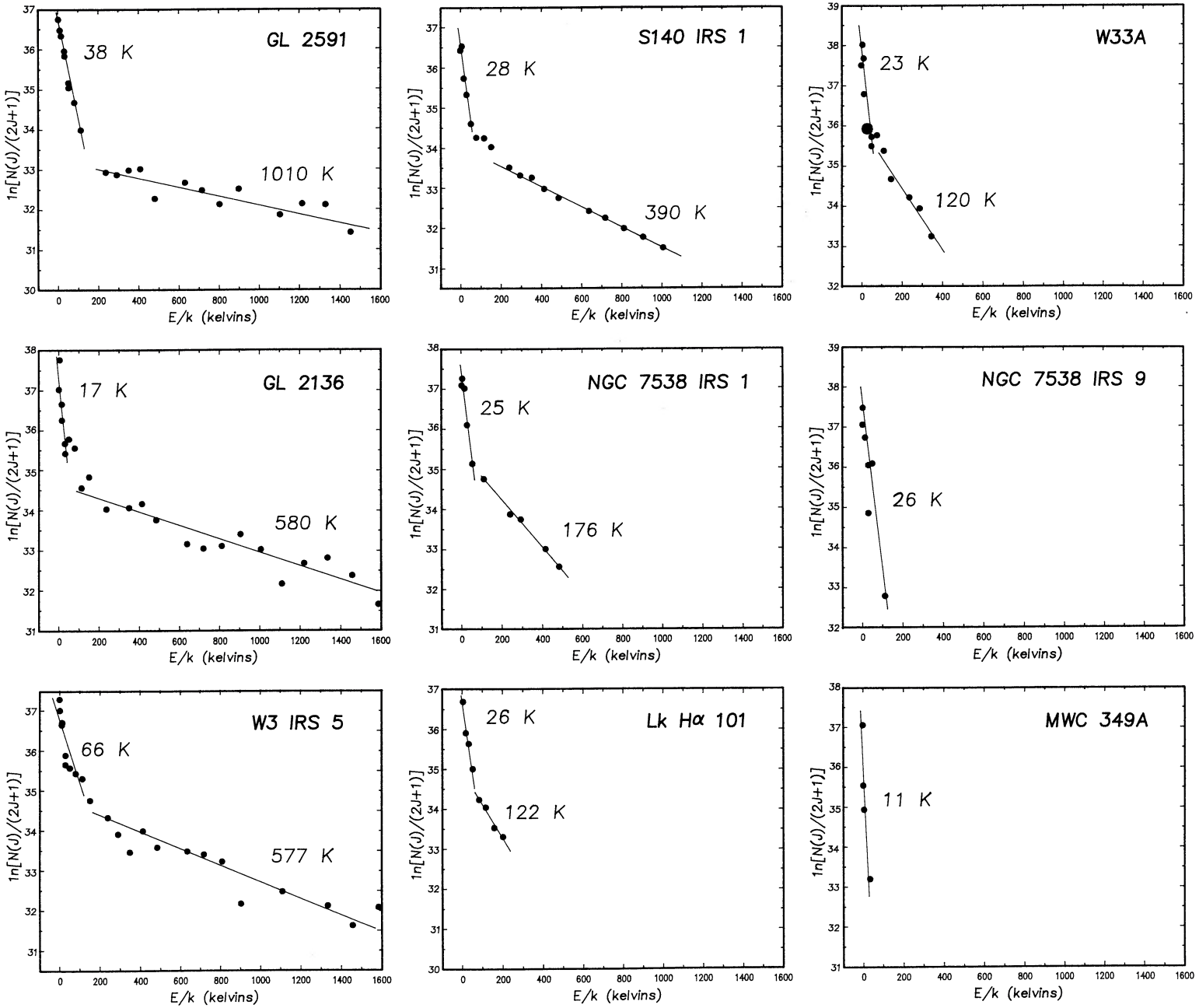

FIG. 9.—CO column densities in each rotational sublevel are plotted as a function of the rotational energy in K for the nine sources. For the sources S140 IRS 1 and LkHα 101, the *R*- and *P*-branch lines were averaged. All plots have the same scale. For the sources GL 2591, GL 2136, W3 IRS 5, S140 IRS 1, NGC 7538 IRS 1, NGC 7538 IRS 9, and W33A, column densities of ^{13}CO are plotted. For the sources LkHα 101 and MWC 349A, column densities of ^{12}CO are used. Separate least-squares fits are made by the low-*J* points and the high-*J* points. The CO rotational temperatures corresponding to the line slopes are shown. In the W33A figure, a larger filled circle indicates the *R*3 and *P*3 lines, each of which yielded the same column density for the $J = 3$ level.

mean line width. As we show below, the high-J lines are formed in hot gas while the low-J lines are formed in cold gas. The two temperature components are likely to be physically distinct and need not share a common line width. We must use, therefore, high velocity resolution CO emission observations as a guide in choosing appropriate line widths.

The sources W33A and GL 2591 have been discussed previously (Mitchell, Allen, and Maillard 1988: Mitchell *et al.* 1989). For LkHα 101 we use the CO ($J = 1$–0) emission-line width of 3.5 km s^{-1} from Redman, Kuiper, and Lorre (1986). For the source MWC 349A, we use 3.4 km s^{-1}, the CO ($J = 1$–0) emission line width found by Knapp *et al.* (1977). For GL 2136, we use the CO ($J = 1$–0) line width of 8 km s^{-1} found by Dinger *et al.* (1979). A choice of line width for the other sources (W3 IRS 5, NGC 7538 IRS 1, NGC 7538 IRS 9, and S140 IRS 1) is difficult because of the complex nature of the CO emission lines. The ^{12}CO ($J = 1$–0) and ^{12}CO ($J = 2$–1) lines are broad (8–14 km^{-1} FWHM), asymmetric, and possess extended, high-velocity wings. The emission-line observations are taken with beam sizes typically in the range 16″–60″, whereas the infrared observations probe essentially a single line of sight. Black and Willner (1984) found very narrow (1.4 km s^{-1}) ^{12}CO ($v = 2$–0) absorption lines toward NGC 2024 IRS 2, which contrast with considerably broader CO rotational emission lines. They suggested as an explanation that, because the source IRS 2 is offset from the cloud center, the infrared line of sight does not probe the same region of the cloud as do the millimeter observations. The sources W3 IRS 5, NGC 7538 IRS 1, NGC 7538 IRS 9, and S140 IRS 1, on the other hand, are located precisely at density maxima in their respective molecular cloud cores. In these cases the absorption line of sight will pass through the regions affected by outflows from the active central objects, and line widths need not be small. We have adopted 6 km s^{-1} for S140 IRS 1, and 8 km s^{-1} for W3 IRS 5, NGC 7538 IRS 1, and NGC 7538 IRS 9.

For each source, a curve-of-growth analysis was carried out, following Spitzer (1978), using the line widths stated above. The result of the analysis is a column density, N_J, for the initial state of each measured transition. If the CO energy levels are populated according to thermodynamic equilibrium, the Boltzmann equation applies, and so $N_J/(2J + 1) \propto \exp(-E_J/kT)$, where E_J is the energy of the Jth rotational state above the ground rotational state. It is, therefore, useful to plot $\ln[N_J/(2J + 1)]$ versus E_J/k. If the data points fall along a straight line, then LTE is probably a valid approximation and the gas temperature is obtained as the inverse of the slope. Figure 9 shows such "Boltzmann" plots, all with the same scale, for the nine sources. The most striking feature of Figure 9 is that, for seven of the sources, a single straight line is a poor representation of the data. The distribution of points, for these sources, shows a break at $E/k \approx 50$–100 K. We see that the low-J points can be fitted by one straight line, while the higher J points can be fitted by a second line of shallower slope. Our interpretation, as made previously for W33A (Mitchell, Allen, and Maillard 1988) and GL2591 (Mitchell *et al.* 1989), is that the low-J absorption lines are formed in cold gas while the high-J absorption lines are formed in hot or warm gas. The lines in Figure 9 are least-squares fits. CO temperatures obtained from Boltzmann's equation are shown. Because the scale of Figure 9 is not appropriate for displaying the cold gas component, we show in Figure 10 Boltzmann plots for the cold gas alone, together with the least-squares fits. From Figures 9 and 10 we see that cold gas (temperatures 11–66 K) is seen in front of all nine sources, while seven out of the nine sources show, in addition, a hot gas component (temperatures 120–1010 K).

The absence, in NGC 7538 IRS 9, of ^{13}CO absorption lines from higher rotational levels suggests that higher J lines of ^{12}CO may be unsaturated in this source. Equivalent width measurements show that this is, indeed, the case. A Boltzmann plot of ^{12}CO in NGC 7538 IRS 9 is shown in Figure 11. Column densities were calculated assuming a line width of 8 km s^{-1}. The line through low-J points in Figure 11 indicates gas with a temperature of 16 K. The high-J lines ($J \geq 4$) show the presence of warm gas at $T = 180$ K. The cold gas temperature deduced from ^{12}CO lines is considerably lower than that obtained using ^{13}CO lines. The low-J lines of ^{12}CO have, however, optical depths up to $\tau = 5$ so that they are at the transition region between the linear and saturated portions of the curve of growth. The column densities deduced from the low-J lines of ^{12}CO will be less reliable than those from the ^{13}CO lines because of the large corrections for optical depth that must be applied to the ^{12}CO lines. We adopt, therefore, the temperature of 26 K for the cold gas in front of NGC 7538 IRS 9, as found from ^{13}CO lines. Higher J lines ($J \geq 4$) of ^{12}CO have optical depths from 1.2 to 2, which puts them on the linear portion of the curve of growth.

Of the eight sources showing hot gas, we believe that seven of the detections are new. The exception is NGC 7538 IRS 1. Wilson *et al.* (1983) have observed emission from NGC 7538 IRS 1 in several rotational transitions of NH_3 having E/k values up to $\approx$400 K. They find a rotational temperature of 170 K, in excellent agreement with our CO rotational temperature of 176 K.

Once an excitation temperature is known, the total CO column density (in the ground vibrational state) can be calculated from the CO column density in any rotational state (of the ground vibrational state) using the Boltzmann equation in the form

$$\frac{N_J}{N} = \frac{g_J}{u(T)} e^{-E_J/kT} .$$

For a given gas component we calculate total CO column densities using each rotational state and average the results. Temperatures and column densities for all sources are listed in Table 5. In the cases of LkHα 101 and MWC 349A, it is necessary to convert ^{12}CO column densities to ^{13}CO column densities. Most recent determinations of the ^{12}C/^{13}C isotope ratio in the local interstellar medium are reasonably consistent with the solar system value of 89. For example, Scoville *et al.* (1983) find ^{12}CO/^{13}CO = 96 in the core of the Orion Molecular Cloud, and Stahl *et al.* (1989) obtain $^{12}CH^+/^{13}CH^+ = 77$ toward ζ Oph. For LkHα 101, MWC 349A, and NGC 7538 IRS 9, therefore, the calculated ^{12}CO column densities were divided by the solar system isotopic abundance ratio, 89, to obtain the ^{13}CO column densities in Table 5. The errors quoted in Table 5 for temperatures and total CO column densities are 1 σ errors due to scatter in the individual N_J's.

It is important to consider the uncertainty in the calculated column densities introduced by uncertainty in the intrinsic line widths. We have used ^{13}CO emission line widths as a guide in selecting the intrinsic widths of ^{13}CO absorption lines. If the emitting gas has an appreciable optical depth in the ^{13}CO emission lines, the emission lines will be broadened. Toward W33A, for example, Goldsmith and Mao (1983) found a ^{13}CO

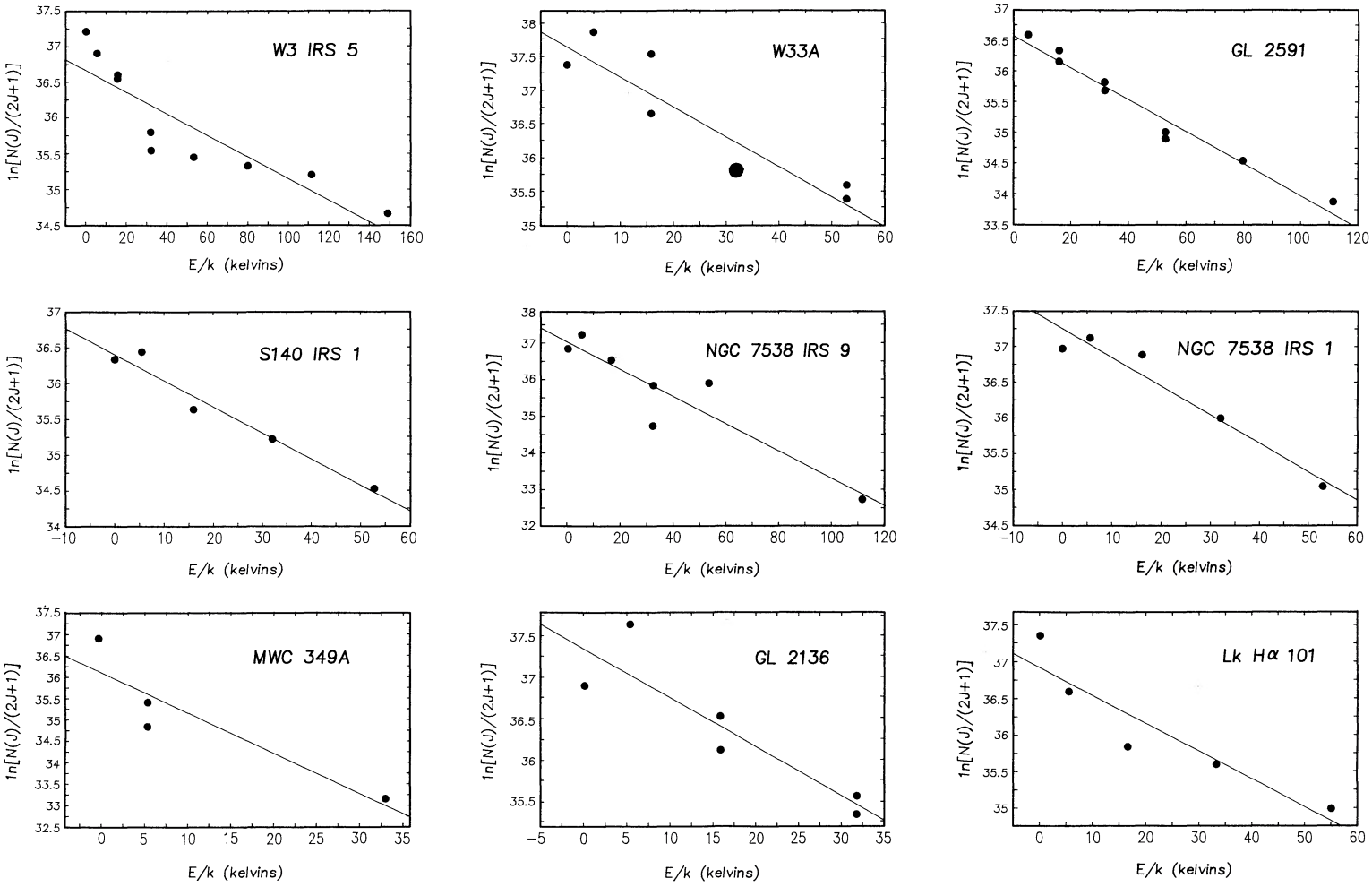

FIG. 10.—Boltzmann plots, as in Fig. 9, but for the lines of low rotational quantum number only

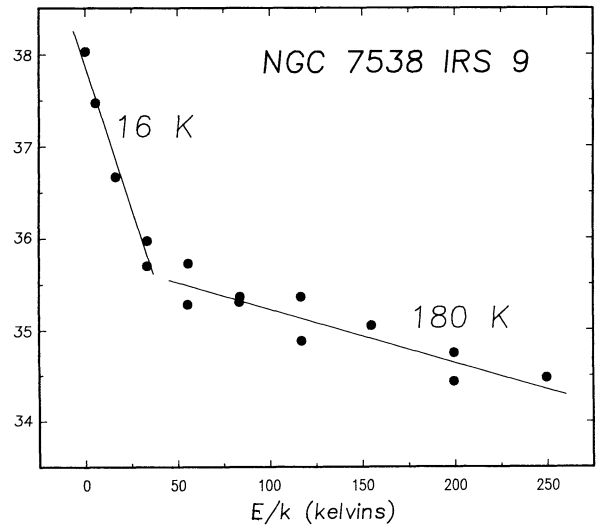

FIG. 11.—A Boltzmann plot, as in Fig. 9, for ^{12}CO lines in NGC 7538 IRS 9

line width of 8 km s^{-1} while Jaffe *et al.* (1984) obtained a width of 5 km s^{-1} for the less abundant $C^{18}O$. To assess the sensitivity of column densities to line width, we have calculated column densities for a range of line widths. A sample of the results is given in Table 6 for the two sources S140 IRS 1 and W3 IRS 5. The first column is the assumed full width at half-maximum. The optical depth of each line comes out of the curve-of-growth calculation. To simplify the presentation in Table 6, we list in columns (2) and (6) an optical depth which is representative of lines with low rotational quantum number ($J \approx 1$), and in columns (4) and (8) an optical depth which is appropriate for lines of high rotational quantum number ($J \approx 15$). The notation N/N_6 indicates the calculated column density divided by the column density for a FWHM of 6 km s^{-1}. The ratio N/N_6 is, therefore, the factor by which the column densities of ^{13}CO toward S140 IRS 1, in Table 5, must be increased if the intrinsic line width is less than 6 km s^{-1}. Similarly, the column densities of ^{13}CO toward W3 IRS 5 in Table 5 must be increased by the factor N/N_8 if the line width is less than 8 km s^{-1}. From the entries in Table 6, it is evident that the low-J lines become highly saturated if line widths are as much as 4 km s^{-1} narrower than our assumed widths. In this case, the cold gas column densities of Table 5 would be lower limits. A decrease of line width by 2 km s^{-1}, on the other hand, results in a moderate 25%–30% increase in the calculated column density of cold gas.

The high-J lines, which are formed in hot gas, have lower optical depth than the lines of low J. The hot gas column densities are, therefore, much less sensitive to the assumed line width. For the examples of S140 IRS 1 and W3 IRS 5 in Table 6, a decrease in line width of 4 km s^{-1} produces a 30% increase in the column density of the hot gas. Higher spectral resolution observations are needed to determine the absorption line widths and resolve the column density uncertainty. An increase in resolution by a factor of 2–3, which is well within the capability of the FT Spectrometer, would settle the issue.

Another complication to the interpretation of the observed line widths is the possible clumpy structure of cloud cores. The line of sight may intersect a number of clumps, so that the observed line width will be due, in part, to the relative motion of the various clumps. If the individual clumps are optically thick, our calculated column densities will be too small.

Limits can be placed on the gas density by exploiting the fact

TABLE 5

^{13}CO TEMPERATURES AND COLUMN DENSITIES

SOURCE	COLD COMPONENT		HOT COMPONENT	
	T (K)	N (cm^{-2}) × 10^{-17}	T (K)	N (cm^{-2}) × 10^{-17}
W33A	23^{+5}_{-4}	2.1 ± 0.9	120^{+14}_{-10}	2.3 ± 0.4
W3 IRS 5	66^{+15}_{-10}	2.2 ± 0.8	577^{+74}_{-59}	2.1 ± 0.7
GL 2136	17^{+5}_{-3}	1.2 ± 0.5	580^{+60}_{-50}	2.5 ± 0.7
GL 2591	38 ± 3	1.2 ± 0.2	1010^{+220}_{-140}	0.93 ± 0.2
NGC 7538/1	25 ± 4	1.5 ± 0.3	176 ± 8	1.4 ± 0.1
NGC 7538/9[a]	26 ± 5	1.6 ± 0.9	180^{+40}_{-30}	0.025 ± 0.0004
S140 IRS 1	28 ± 3	0.51 ± 0.1	390 ± 10	0.73 ± 0.05
LkHα 101[a]	26 ± 6	0.013 ± 0.004	122^{+20}_{-15}	0.0068 ± 0.0005
MWC 349A[a]	11^{+5}_{-3}	0.0034 ± 0.0022	...	...

[a] For LkHα 101 and MWC 349A, temperatures and column densities were obtained using lines of ^{12}CO. For NGC 7538 IRS 9, the temperature and column density of the hot component were obtained using lines of ^{12}CO. The column densities listed in the table are the ^{12}CO column densities divided by 89, the assumed $^{12}CO/^{13}CO$ abundance ratio.

TABLE 6

SENSITIVITY OF ^{13}CO COLUMN DENSITIES TO LINE WIDTHS

$\Delta v_{1/2}$ (km s^{-1}) (1)	S140 IRS 1				W3 IRS 5			
	τ(low-J) (2)	N/N_6 (3)	τ(high-J) (4)	N/N_6 (5)	τ(low-J) (6)	N/N_8 (7)	τ(high-J) (8)	N/N_8 (9)
2.0.....	>10	10	1	1.3	...	...	...	...
4.0.....	2	1.3	<1	1.1	≥10	2.5	1	1.3
6.0.....	1	1	<1	1	3	1.2	<1	1.1
8.0.....	...	...	...	...	2	1	<1	1

that a Boltzmann distribution of rotational populations is maintained out to some rotational level. The hot gas properties are further discussed in § VII. Here we address the cold component only. The largest J level detectable in the cold gas varies from $J = 3$ for GL 2136 and MWC 349A, to $J = 7$ in W3 IRS 5. Viscuso and Chernoff (1988) have calculated CO rotational level populations for a range of temperatures (10–10^3 K) and densities (10^3–10^7 cm^{-3}). Using their Figure 4, we can find the minimum gas density which will maintain LTE in the observed range of J levels. The result is the same for all sources, namely that the density of the cold gas must exceed 10^5 cm^{-3}.

IV. COMPARISON WITH CO AND NH_3 EMISSION-LINE RESULTS

a) Temperature

It is of interest to compare the temperatures of the cold gas, determined here, with other temperature measurements. Perhaps the most widely used method for obtaining gas kinetic temperatures in dense clouds is through the measurement of emission from low-lying rotational states of ^{12}CO. The transitions CO ($J = 1$–0) and CO ($J = 2$–1) have been frequently employed. The procedure is straightforward in principle. The antenna temperature, T_A^*, is corrected for the coupling efficiency to the source and for the forward spillover and scattering efficiency to yield the radiation temperature, T_R. The kinetic temperature is obtained from T_R by assuming that the optical depth in the transition is large and that the CO energy levels are thermalized. Errors in the deduced temperatures can arise from uncertain coupling efficiencies, which depend on the source intensity distribution within the beam, and from possible self-absorption in the very strong lines.

Ammonia is a second useful interstellar thermometer. Observations of two or more inversion transitions of NH_3 provide a rotational temperature. The assumption that the ammonia is collisionally excited by H_2 permits a calculation of the kinetic temperature.

In Table 7, the ^{13}CO temperatures of the cold gas, determined from the absorption spectra presented in this paper, are compared to temperatures found by other methods. CO temperatures of NGC 7538 and S140 are taken from Wu and Evans (1989), who carried out a careful reanalysis of the gas and dust temperatures of several dense clouds. The ammonia temperatures in Table 7 are taken from Danby *et al.* (1988), who recalibrated the relationship between rotational and kinetic temperatures using new calculations of collisional excitation rates of NH_3 by H_2. The NH_3 rotational temperatures, from which the kinetic temperatures are derived, are from Takano (1986). The gas temperatures toward W3 IRS 5 and GL 2591 were deduced from CO ($J = 2$–1) observations obtained by Mitchell and Hasegawa in 1989 August, using the James Clerk Maxwell Telescope[6] on Mauna Kea (Mitchell and Hasegawa 1990). We have deduced kinetic temperatures from the peak antenna temperatures as outlined above, employing a beam efficiency of 0.79 and assuming uniform source temperatures within the 20″ beam. The results are given in Table 7 with the reference "unpublished JCMT data." A temperature for the W3 cloud, based on continuum observations at 1.3 and 3 mm (Gordon 1987), is included in Table 7. The sources LkHα 101, MWC 349A, and GL 2136 are missing from Table 7 because we could not find reliable temperatures in the literature.

[6] The JCMT is operated by the Royal Observatory, Edinburgh on behalf of the United Kingdom Science and Engineering Research Council, the National Research Council of Canada, and the Netherlands Organisation for Pure Research.

TABLE 7

TEMPERATURE OF THE COLD COMPONENT COMPARED WITH OTHER MEASUREMENTS

Source	T (CO absorption)	T (other)	Method	References
W33A	23	26	CO 2–1	1
W3 IRS 5	66	65	Dust emission	2
		67	CO 2–1	3
GL 2591	38	37	NH_3	4
		44	CO 2–1	3
NGC 7538 IRS 9 ...	26	35	NH_3	4
		24	CO 2–1	5
		26	CO 1–0	5
NGC 7538 IRS 1 ...	25	35	NH_3	4
		24	CO 2–1	5
		26	CO 1–0	5
S140 IRS 1	28	30	NH_3	4
		27	CO 2–1	5
		30	CO 1–0	5

REFERENCES.—(1) Goldsmith and Mao 1983; (2) Gordon 1987; (3) Unpublished JCMT data; (4) Danby *et al.* 1988; (5) Wu and Evans 1989.

The temperatures deduced from CO emission and absorption lines are generally in good agreement. One implication of the agreement is that the line widths we have used in the curve of growth analyses are reasonable. Smaller line widths would steepen the point distribution in plots such as Figure 9, resulting in lower calculated temperatures. The steepening occurs because level population is inversely proportional to the rotational quantum number, J, so that the opacity corrections (i.e., increases) to N_J are also inversely proportional to J.

The temperatures from NH_3 are in good agreement with CO absorption temperatures for GL 2591 and S140. The two methods do not, however, give consistent results for NGC 7538, the ammonia temperature being about 30% higher. In the W3 core, the dust temperature from continuum observations (Gordon 1987) is essentially identical to the gas temperature deduced from CO absorption lines.

The close agreement between ^{13}CO absorption temperatures and ^{12}CO emission temperatures is surprising. The large optical depth in ^{12}CO low-J emission lines implies that the emitting gas is further from the infrared source than is the ^{13}CO absorbing gas. The agreement between CO absorption and emission temperatures may be related to another remarkable agreement, that between the dust temperature from 60 and 100 μm *IRAS* observations, and gas kinetic temperatures from CO(1–0) and CO(2–1) emission lines (Wu and Evans 1989). The latter agreement does not appear to be understood. Possible simplified structures might be envisioned for the cloud cores. First, a hot circumstellar shell or disk may be surrounded by a sphere of uniform, low-temperature gas. In this picture, ^{13}CO absorption lines of high J are formed as the continuous radiation passes through the hot gas, while the observed low-J absorption lines are formed in the cooler surrounding gas. The optically thick CO emission comes from the outer layers of the colder region. A second physical model is of a cloud possessing a continuous gradient in temperature and density. High-J absorption lines of ^{13}CO will be preferentially formed in the inner, hotter regions because of the larger population of excited CO. Low-J absorption lines will form in the outer, cooler regions. Again, the temperature agreement

between ^{12}CO low-J emission lines and ^{13}CO low-J absorption lines is qualitatively understandable. It may be possible to distinguish between a two-zone model and a cloud with a gradient in temperature and density by making the simplifying assumption of local thermodynamic equilibrium. For example, the adoption of power laws for the density and temperature distribution permits the column density in any J level to be evaluated analytically (assuming LTE). Simple physical models will be, however, of questionable validity for the sources discussed in this paper because of the presence of molecular outflows and the probable clumpiness of the gas. It will be necessary to treat each source separately and in detail, combining the new CO absorption results with the large body of existing emission line data.

b) Column Densities

For several of our sources, ^{13}CO column densities have been determined from ^{13}CO radio emission-line intensities. The basis of the method lies in combining ^{12}CO and ^{13}CO spectral line data to determine the optical depth in the ^{13}CO transition. The column density of ^{13}CO is then calculated, assuming that level populations are in LTE. The method is described in, for example, Margulis and Lada (1985). For dense molecular clouds, the optical depth of ^{13}CO, at the line centers, can be considerable ($\tau_{13} \geq 1$), leading to large uncertainties in the calculated column densities. Self-absorption in ^{12}CO is another source of error in τ_{13} and, therefore, in column densities.

Column densities of ^{13}CO from emission lines are compared, in Table 8, with ^{13}CO column densities from the infrared absorption lines. Column densities of the cold component, the hot component and the total column density (cold plus hot) are given in Table 8. For GL 2591 and NGC 7538 IRS 9 we have calculated new ^{13}CO column densities using ^{12}CO ($J = 2$–1) and ^{13}CO ($J = 2$–1) spectra acquired at the JCMT in 1989 August (Mitchell and Hasegawa 1990). The column density of ^{13}CO toward S140 IRS 1 was calculated by us from spectra published in Hayashi *et al.* (1987).

Emission from low rotational levels will probably be from the cold gas only, so that it is appropriate to compare the emission column densities with the column densities of the cold gas detected in absorption. The agreement is reasonably good. Close agreement between our absorption column densities and column densities obtained from emission lines cannot be expected for a number of reasons. Emitted radiation comes from both foreground and background gas, while absorption lines are produced in the foreground gas only. Also, our extremely narrow beam (which is the subarcsecond size of the IR continuum source) compared to the radio beam should weight our observations toward denser gas. Furthermore, self-absorption in ^{12}CO emission lines will result in ^{13}CO optical depths which are too large and, therefore, in column densities which are too large.

TABLE 8

^{13}CO COLUMN DENSITIES: ABSORPTION AND EMISSION MEASUREMENTS COMPARED

	$N(^{13}CO) \times 10^{-17}$ cm^{-2}				
	Absorption				References for Emission Data
Source	Cold	Hot	Total	Emission	
W33A	2.1	2.3	4.4	1.0	1
W3 IRS 5	2.2	2.1	4.3	3.4	2
GL 2591	1.2	0.93	2.1	2.4	3
NGC 7538 IRS 9	1.6	0.025	1.6	0.63	3
S140 IRS 1	0.51	0.73	1.2	1.4	4

REFERENCES.—(1) Goldsmith and Mao 1983; (2) Hayashi *et al.* 1989; (3) Unpublished JCMT data; (4) Hayashi *et al.* 1987.

V. CORRELATION BETWEEN ^{13}CO COLUMN DENSITY AND SILICATE OPTICAL DEPTH

An absorption feature at 9.7 μm, seen in the spectra of many highly reddened infrared sources, is generally attributed to interstellar grains of silicate composition. If silicate grains are smoothly distributed in molecular gas, the silicate optical depth should be a measure of total gas column density. That is, $\tau(9.7\ \mu m)$ and $N(H_2)$ should be closely correlated. It is quite well established on observational and theoretical grounds that, in strongly shielded regions (i.e., $A_V \geq 4$), CO is an excellent tracer of H_2, with $^{12}CO/H_2 \approx 10^{-4}$. The ^{13}CO column densities of Table 5 provide, therefore, an opportunity to investigate the distribution of silicate grains and molecular gas along the same lines of sight in different molecular clouds. Willner *et al.* (1982) have obtained silicate optical depths, in a uniform fashion, for seven of the nine sources in Table 5, namely for W33A, W3 IRS 5, GL 2136, GL 2591, NGC 7538 IRS 1, NGC 7538 IRS 9, and S140 IRS 1. Figure 12 is a plot of ^{13}CO column density from Table 5 against 9.7 μm optical depth from Willner *et al.* (1982). The ^{13}CO shown is the cold component only. It is not immediately obvious whether the cold gas column density or the total gas column density (cold plus hot) should better correlate with τ(Si). We know neither the origin nor the spatial distribution of the hot gas, so there is no certainty that the ratio of molecular gas to grains is similar to that in the cold gas. Figure 12 shows that the column density of cold ^{13}CO is quite strongly correlated with the silicate optical depth, the correlation coefficient being 0.86. The correlation between τ(Si) and the total ^{13}CO column density is only slightly weaker, with a correlation coefficient of 0.78.

VI. THE RATIO OF SOLID TO GASEOUS CO

An absorption feature at 4.67 μm (2140 cm^{-1}), due to CO in the solid phase, is seen in the spectra of many infrared sources

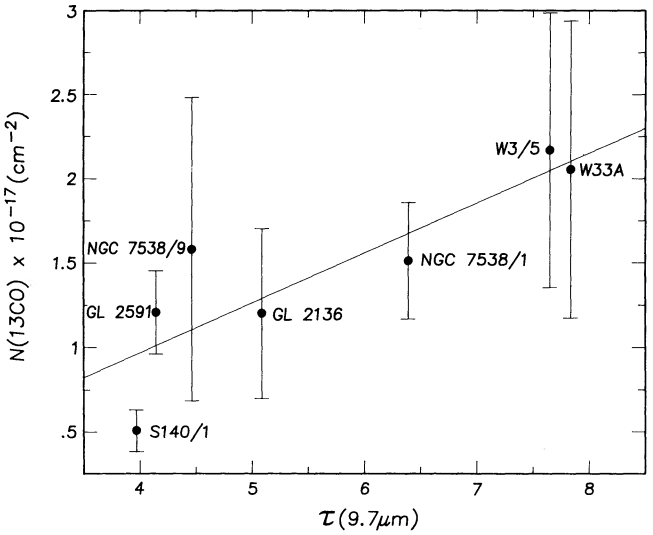

FIG. 12.—The column density of cold ^{13}CO is plotted against the optical depth of the silicate absorption feature for seven sources. The error bars are the 1 σ errors from Table 5. The correlation coefficient, R, is 0.86.

embedded in molecular clouds (Lacy *et al.* 1984; Larson *et al.* 1985; Whittet, Longmore, and McFadzean 1985; Geballe 1986). Of the sources in the present study, solid CO has been found in W33A, NGC 7538 IRS 9, NGC 7538 IRS 1, W3 IRS 5, and GL 2136, while upper limits to the solid CO optical depth exist for GL 2591 and LkHα 101. Because of the relatively small gas column density to LkHα 101, the solid CO upper limit is not very interesting, and we exclude this source from the discussion below. Since the solid and gaseous CO absorption features are seen at the same wavelength, the location of the background continuum (i.e., the surface of last scattering) is identical for the two sets of data. Thus, the gas phase CO occupies precisely the same line of sight as the solid CO. We can, therefore, compare the gas phase and solid phase abundances to determine the fraction of CO which is frozen out onto grains. The result for W33A has been reported previously (Mitchell, Allen, and Maillard 1988), where it was shown that, for this line of sight, solid CO comprises only a few percent of the total CO. It is important to know whether the result for W33A is general.

For the five sources W33A, NGC 7538 IRS 9, NGC 7538 IRS 1, W3 IRS 5, and GL 2136, we have taken solid CO abundances from Sandford *et al.* (1988), who use observational data of Lacy *et al.* (1984) and Geballe (1986). The CO solid-to-gas ratio is given in Table 9 for the cold gas alone and for the total gas column, cold gas plus hot gas. Note that the solid to gas ratio for W33A in Table 9 differs from that reported in Mitchell, Allen, and Maillard (1988) only because of a different assumed $^{12}CO/^{13}CO$ ratio. Those authors adopted $^{12}CO/^{13}CO = 60$, while we use here the solar value, $^{12}CO/^{13}CO = 89$.

It is most unlikely that solid CO can survive in the hot gas toward W3 IRS 5, GL 2136, and GL 2591 at temperatures of $\approx$600–1000 K. For these three cases, the ratio N_{solid}/N_{gas}(cold) should be the preferred measure for the local solid/gas ratio along these lines of sight. The hot gas temperatures for W33A and 6GC 7538 IRS 1 are low enough that the survival of solid CO in ice mixtures cannot be ruled out.

The source NGC 7538 IRS 9 is of particular interest because it has the largest known solid CO column density. The CO solid-to-gas abundance ratio in the line of sight to NGC 7538 IRS 9 is 0.10, the largest in the present sample. It is noteworthy that the nearby source, NGC 7538 IRS 1, has a low solid-to-gas ratio of 0.03. The two sources are embedded in the same molecular cloud, having a separation of only 0.8 pc (if the distance is 2.7 kpc). The different solid CO abundances in front of IRS 9 compared to IRS 1 may imply that most of the observed solid CO is close to the embedded sources rather than being distributed throughout the molecular cloud.

In four of the six sources in Table 9, less than 1% of the observed CO is in the solid state. This contrasts with the results of Whittet, Longmore, and McFadzean (1985) for the Taurus dark cloud complex. They find solid CO in five infrared sources, with the fraction of solid CO as great as 40%. The gas phase abundances used by Whittet, Longmore, and McFadzean (1985) are taken from Frerking, Langer, and Wilson (1982), who employed a telescope with the large beamwidth of 1.6 at the CO ($J = 1$–0) frequency. Beam dilution may, therefore, explain part of the difference between the Taurus results and the results for the sources in Table 9. The determination of gas phase CO abundances toward the Taurus sources by the absorption method would be useful. It may be significant that the temperature of the gas in the Taurus cloud is about 10 K, whereas the temperatures of the cloud cores observed in the present paper are considerably higher (see Table 5). Possibly the accretion of CO onto grains is more rapid at the colder temperatures of the Taurus cloud.

VII. THE HOT GAS

The absorption technique probes a single line of sight to the embedded infrared object, so that we are unable to determine directly the spatial distribution of the hot gas. In the case of GL 2591, we have argued (Mitchell *et al.* 1989) that the hot gas is of such high density that it must be very near the central object. The argument is twofold: First, a Boltzmann distribution of rotational populations is maintained for rotational quantum numbers, J, as high as 23. For optically thin lines (and the observed high-J transitions are optically thin) densities exceeding 10^7 cm^{-3} are required. Second, absorption lines from ^{12}CO in the first excited vibrational state are seen in the spectrum of GL 2591. The excitation temperature of the vibrationally excited CO is consistent with that of the (hot) ground vibrational state CO, implying that the $v = 1$–2 lines are formed in the same gas as the $v = 0$–1 lines. The spontaneous decay rates from $v = 1$ to $v = 0$ are so fast that gas densities exceeding 10^{10} cm^{-3} are required to maintain an observable population in the first excited vibrational state. With such high densities, the 1010 K gas in GL 2591 must be a shell, disk, or extended atmosphere very close to the YSO. ^{12}CO $v = 1$–2 lines are seen also in GL 2136, so that the same arguments apply for GL 2136.

In W3 IRS 5 and S140 IRS 1, no $v = 1$–2 transitions are seen, but the Boltzmann distribution of rotational states out to high J again implies $n \geq 10^7$ cm^{-3}. It seems plausible, by

TABLE 9

^{12}CO SOLID TO GAS RATIO[a]

Source	N_{solid} ($\times 10^{-17}$)	N_{gas}(cold) ($\times 10^{-19}$)	N_{solid}/N_{gas}	N_{gas}(all) ($\times 10^{-19}$)	N_{solid}/N_{gas}(all)
W33A	7.4	1.9	0.04	3.9	0.02
NGC 7538 IRS 9	14.5	1.4	0.10	1.4	0.10
NGC 7538 IRS 1	0.76	1.3	0.006	2.5	0.003
W3 IRS 5	0.83	2.2	0.004	4.3	0.002
GL 2136	0.62	1.0	0.006	3.2	0.002
GL 2591	<0.4	1.1	<0.004	1.9	< 0.002

[a] The ^{12}CO gas column densities are obtained from the ^{13}CO column densities (of Table 3) by multiplying by the abundance ratio, $^{12}CO/^{13}CO = 89$. The abundances of solid CO are taken from Sandford *et al.* 1988. Column densities are in units of cm^{-2}.

analogy with GL 2591 and GL 2136, that the hot gas toward W3 IRS 5 and S140 IRS 1 is also very close to the embedded sources. For the remaining four sources, NGC 7538 IRS 1, NGC 7538 IRS 9, LkHα 101, and W33A, densities as low as 10^6 cm^{-3} are permitted for the hot gas so that a more widespread distribution is possible.

Recent observations of high-J lines of CO ($J = 7$ and higher) in emission have led to the detection of hot gas in several molecular clouds (Jaffe, Harris, and Genzel 1987; Harris *et al.* 1987; Stutzki *et al.* 1989). Gas with temperatures of 100–500 K was found in the cloud cores of M17, S106, W51, and DR 21. In W51 and DR 21, the hot gas is associated with the H II regions of each source and has a spatial extent of about 1 pc. Harris *et al.* (1987) suggest that the gas is heated by photoelectrons ejected from grains by 912 Å to 1100 Å photons from adjacent young, hot stars. The column density of hot gas is too large by factors of 10–100 to be produced in a single photodissociation region (e.g., Tielens and Hollenbach 1985). Harris *et al.* (1987) invoke, therefore, a model in which the cloud is clumpy, so that ultraviolet photons penetrate deeply into the cloud core. The observed column of hot gas is, in this picture, the sum of many clump interfaces along the line of sight. A radiation field enhanced by a factor of $\approx 10^5$ over the mean interstellar radiation field is required for the model to yield the observable column density of gas with a temperature of several hundred degrees. There is not yet any overlap in the sources with hot gas seen in absorption and sources with hot gas seen in emission. An important task for the future is to map these sources in high excitation emission lines to put direct constraints on the spatial extent of the hot gas.

If the hot gas is close to the central source and is heated by it via gas-grain collisions (Scoville and Kwan 1976), a crude estimate of the size of the hot region can be found by determining the distance from the central source at which the grain temperature equals the observed gas temperature. We have carried out this exercise for the seven sources which have a component of hot gas, with the results shown in Table 10. The dust temperatures were obtained using an expression given in Takano (1986) based on Scoville and Kwan (1976). The source luminosities are based on often poorly known distances, introducing an additional uncertainty. We see from Table 10 that the grain heating assumption requires the hot gas to be at a distance of ≈ 10 AU from GL 2591, ≈ 100 AU from W3 IRS 5, GL 2136, and S140 IRS 1, and ≈ 1000 AU from W33A, NGC 7538 IRS 1, NGC 7538 IRS 9, and LkHα 101.

TABLE 10

DISTANCE FROM THE EMBEDDED SOURCES AT WHICH THE DUST TEMPERATURE EQUALS THE TEMPERATURE OF THE HOT GAS COMPONENT

Source	$L/L_\odot$	T (K)	Distance (AU)
W33A	3×10^4	120	1900
W3 IRS 5	4.2×10^5	577	140
GL 2136	1.8×10^5	580	91
GL 2591	1.6×10^4	1010	6.7
NGC 7538/1	1.5×10^5	176	1630
NGC 7538/9	3×10^4	180	2000
S140/1	2.4×10^4	390	89
LkHα 101	1.2×10^4	122	1150

VII. SUMMARY

High-resolution (8 km s^{-1}), M band (4.7 μm) spectra have been presented for the seven embedded infrared sources W3 IRS 5, S140 IRS 1, NGC 7538 IRS 1, NGC 7538 IRS 9, GL 2136, LkHα 101, and MWC 349A. Properties of the foreground gas were deduced using absorption lines of the fundamental vibrational band of ^{13}CO and ^{12}CO. The data from these seven objects were combined with previously published work for W33A and GL 2591, with the following results:

1. Cold CO is seen toward all nine sources, with temperatures from 11 K (for MWC 349A) to 66 K (for GL 2591). Column densities of cold CO are presented. To achieve the observed Boltzmann population of low rotational levels, the density of the cold gas must exceed $\approx 10^5$ cm^{-3}.
2. Hot gas is seen toward eight of the nine objects, with temperature from 120 K (for W33A) to 1010 K (for GL 2591). With the exception of NGC 7538 IRS 1, we believe that the hot gas detections are new. Lower limits to the hot gas density were obtained. The presence of ^{12}CO ($v = 1$–2) lines in the spectra of GL 2591 and GL 2136 requires a density greater than 10^{10} cm^{-3}. In W3 IRS 5 and S140 IRS 1, the Boltzmann distribution of high-J populations of the fundamental band of ^{13}CO implies that the density of the hot gas exceeds 10^7 cm^{-3}. A similar argument for NGC 7538 IRS 1, NGC 7538 IRS 9, W33A, and LkHα 101 implies that the hot gas density is greater than 10^6 cm^{-3}.
3. The hot gas toward GL 2591, GL 2136, W3 IRS 5, and S140 IRS 1 is probably very near the central source and heated via gas-grain collisions. For the sources NGC 7538 IRS 1, NGC 7538 IRS 9, LkHα 101, and W33A, a more spatially extended distribution for the hot gas, such as in photodissociation regions, cannot be excluded.
4. The optical depth in the silicate (9.7 μm) feature is strongly correlated with the ^{13}CO column density, confirming that silicate optical depth is a useful measure of gas column density.
5. The ratio of solid-to-gaseous CO is obtained for seven sources using published solid CO column densities. In the gas toward NGC 7538 IRS 9 and W33A, the fraction in solid form is moderately high (4% and 10%, respectively). Less than 1% of CO is in solid form along the four other lines of sight. Our results do not agree with those of Whittet, Longmore, and McFadzean (1985) who found solid CO fractions as high as 40% for the Taurus dark cloud. The difference, if real, may be due to the lower temperature (10 K) of the Taurus cloud.

We thank the staff of the CFHT for its support. G. F. M. is grateful for the hospitality he received during a sabbatical year at the CFHT Corporation in Waimea, where this paper was written. This research program was supported in part by an operating grant from the Natural Sciences and Engineering Research Council of Canada (to G. F. M.).

REFERENCES

Bally, J., and Lada, C. J. 1983, *Ap. J.*, **265**, 824.
Black, J. H., and Willner, S. P. 1984, *Ap. J.*, **279**, 673.
Danby, G., Flower, D. R., Valiron, P. Schilke, P., and Walmsley, C. M. 1988, *M.N.R.A.S.*, **235**, 229.
Dinger, A., Dickinson, D. F., Gottlieb, C. A., and Gottlieb, E. W. 1979, *Pub. A.S.P.*, **91**, 830.
Frerking, M. A., Langer, W. D., and Wilson, R. W. 1982, *Ap. J.*, **262**, 590.
Geballe, T. R. 1986, *Astr. Ap.*, **162**, 248.
Goldsmith, P. F., and Mao, X.-J. 1983, *Ap. J.*, **265**, 1983.
Gordon, M. A. 1987, *Ap. J.*, **316**, 258.
Hamann, F., and Simon, M. 1986, *Ap. J.*, **311**, 909.
———. 1988, *Ap. J.*, **327**, 876.
Harris, A. I., Stutzki, J., Genzel, R., Lugten, J. B., Stacey, G. J., and Jaffe, D. T. 1987, *Ap. J. (Letters)*, **322**, L49.

Hayashi, M., Hasegawa, T., Omodaka, T., Hayashi, S. S., and Miyawaka, R. 1987, *Ap. J.*, **312**, 327.
Hayashi, M., Kobayashi, H., and Hasegawa, T. 1989, *Ap. J.*, **340**, 298.
Jaffe, D. T., Genzel, R., Harris, A. I., Lugten, J. B., Stacey, G. J., and Stutzki, J. 1989, *Ap. J.*, **344**, 265.
Jaffe, D. T., Harris, A. I., and Genzel, R. 1987, *Ap. J.*, **316**, 231.
Jaffe, D. T., Hildebrand, R. H., Keene, J., Harper, D. A., Loewenstein, R. F., and Moran, J. M. 1984, *Ap. J.*, **281**, 281.
Kameya, O., Hasegawa, T. I., Hirano, N., Takakubo, K., and Seki, M. 1989, *Ap. J.*, **339**, 222.
Knapp, G. R., Kuiper, T. B. H., Knapp, S. L., and Brown, R. L. 1977, *Ap. J.*, **214**, 78.
Lacy, J. H., Baas, F., Allamandola, L. J., Persson, S. E., McGregor, P. S., Lonsdale, C. J., Geballe, T. R., and van de Bult, C. E. P. 1984, *Ap. J.*, **276**, 533.
Larson, H. P., Davis, D. S., Black, J. H., and Fink, U. 1985, *Ap. J.*, **299**, 873.
Margulis, M., and Lada, C. J. 1985, *Ap. J.*, **299**, 925.
Mitchell, G. F., Allen, M., Beer, R., Dekany, R., Huntress, W., and Maillard, J.-P. 1988*a*, *Astr. Ap.*, **201**, L16.
———. 1988*b*, *Ap. J. (Letters)*, **327**, L17.
Mitchell, G. F., Allen, M., and Maillard, J.-P. 1988, *Ap. J. (Letters)*, **333**, L55.
Mitchell, G. F., Belcourt, K., Maillard, J.-P., and Allen, M. 1990, in *Submillimetre Astronomy*, ed. G. D. Watt and A. S. Webster (Dordrecht: Kluwer), p. 187.
Mitchell, G. F., Curry, C., Maillard, J.-P., and Allen, M. 1989, *Ap. J.*, **341**, 1020.
Mitchell, G. F., and Hasegawa, T. I. 1990, in preparation.
Redman, R. O., Kuiper, T. B. H., and Lorre, J. J. 1986, *Ap. J.*, **303**, 300.
Sandford, S. A., Allamandola, L. J., Tielens, A. G. G. M., and Valero, G. J. 1988, *Ap. J.*, **329**, 498.
Scoville, N. Z., Hall, D. N. B., Kleinmann, S. G., and Ridgway, S. T. 1983, *Ap. J.*, **275**, 201.
Scoville, N. Z., and Kwan, J. 1976, *Ap. J.*, **206**, 718.
Simon, M., and Cassar, L. 1984, *Ap. J.*, **283**, 179.
Spitzer, L., Jr. 1978, *Physical Processes in the Interstellar Medium* (New York: Wiley).
Stahl, O., Wilson, T. L., Henkel, C., and Appenzeller, I. 1989, *Astr. Ap.*, **221**, 321.
Stutzki, J., Stacey, G. J., Genzel, R., Harris, A. I., Jaffe, D. T., and Lugten, J. B. 1988, *Ap. J.*, **332**, 379.
Takano, T. 1986, *Ap. J.*, **303**, 349.
Tielens, A. G. G. M., and Hollenbach, D. J. 1985, *Ap. J.*, **291**, 722.
Viscuso, P. J., and Chernoff, D. F. 1988, *Ap. J.*, **327**, 364.
White, R. L., and Becker, R. H. 1985, *Ap. J.*, **297**, 677.
Whittet, D. C. B., Longmore, A. J., and McFadzean, A. D. 1985, *M.N.R.A.S.*, **216**, 45P.
Willner, S. P., *et al.* 1982, *Ap. J.*, **253**, 174.
Wilson, T. L., Mauersberger, R., Walmsley, C. M., and Batrla, W. 1983, *Astr. Ap.*, **127**, L19.
Wu, Y., and Evans, N. J., II. 1989, *Ap. J.*, **340**, 307.

MARK ALLEN: Jet Propulsion Laboratory, M/S 183-601, 4800 Oak Grove Drive, Pasadena, CA 91109

REINHARD BEER: Jet Propulsion Laboratory, M/S 183-301, 4800 Oak Grove Drive, Pasadena, CA 91109

KENNETH BELCOURT and GEORGE F. MITCHELL: Department of Astronomy, Saint Mary's University, Halifax, N.S., Canada, B3H 3C3

JEAN-PIERRE MAILLARD: Institut d'Astrophysique, 98 bis, boulevard Arago, F-75014, Paris, France